ANALYTICAL AND FEM MODELING OF ALUMINUM BILLET INDUCTION HEATING WITH EXPERIMENTAL VERIFICATION

Mark W. Kennedy [1], Shahid Akhtar [1], Jon Arne Bakken [1] and Ragnhild E. Aune [1,2]
[1] Dept. of Material Science and Engineering, Norwegian University of Science and Technology (NTNU)
N-7491 Trondheim, Norway.
[2]Dept. of Materials Science and Engineering, Royal Institute of Technology (KTH)
S-100 44 Stockholm, Sweden.

Communicating author: ragnhild.aune@ntnu.no

Keywords: Ceramic Foam Filters, CFF, electromagnetic, filtration

Abstract

Induction heating is commonly used in the re-heating of aluminum billets before forging or extrusion. Powerful finite element modeling (FEM) tools are available to assist in the design of such processes; however, such models should be validated by comparison with analytical solutions or experimental results to ensure accuracy.

Induction heating experiments have been performed using a number of different coil designs and work piece dimensions at 50 Hz. Aluminum alloys with different electrical conductivities have been used, i.e. 6060 and A356. Process parameters such as: current, power, magnetic field, electrical conductivity, etc. have been measured with high precision instrumentation. Experimental data are presented and compared with equivalent 1D analytical and 2D axial symmetric FEM modeling results.

The effect of frequency on the induction heating process is reviewed using the validated analytical and FEM models. Some recommendations are given with respect to appropriate modeling techniques, boundary conditions and numerical mesh sizes.

Introduction

Induction heating is produced by the circular eddy currents within a work piece. These currents are driven by the time varying magnetic flux density in the air-gap between the work piece and the coil. The eddy currents are concentrated in the outermost layer or first electromagnetic penetration depth (δ_w) and circulate in a direction opposing the magnetic field produced by the coil.

Accurate estimation of the magnetic field strength in the air-gap is critical for the correct estimation of the heating rate (power) developed in the work piece. Coils used for induction heating typically have a diameter similar in magnitude to their length. Magnetic fields produced by such 'short' coils, can not be accurately estimated using a long coil formula such as Equation (1):

$$\left|\overrightarrow{B_\infty}\right| = \frac{\mu_o \mu_r N_c I_c}{l_c} \qquad (1)$$

where B_∞ is the axial flux density of an infinite coil [T], μ_o the magnetic permeability of the free space (4π x10^{-7} [H/m]), μ_r the relative magnetic permeability, N_c the number of coil turns, I_c the coil RMS current [A], and l_c the length of the coil [m].

Equation (1) can be used with a 'short coil' correction factor, to estimate the average z-component of the magnetic flux density of an empty short coil with high precision.

In 1909 Nagaoka [1] first published a correction factor k_N, to six significant digits, which contains the solutions to the double elliptical integrals of Lorenz [2]. The method of Knight [3] as indicated in Equation (2), gives k_N to approximately three significant figures. Equation (2) is sufficiently accurate for most induction furnace calculations. k_N can also be computed using numerical equation solvers to single or double precision [4].

$$k_N = \frac{1}{1 + 0.4502\left(\frac{D_c + \delta_c}{l_c}\right)} \qquad (2)$$

where D_c the inside diameter of the coil [m], and δ_c the electromagnetic penetration depth into the coil [m].

To have less than a 5% error (i.e. a k_N >0.95) in applying Equation (1) without a short coil correction factor, a coil needs to be ~10 times as long as its diameter. This can be found by evaluating Equation (2). From Equation (2), a typical induction coil with a 1:1 ratio of diameter to height, would have <70% of the theoretical magnetic flux density in the z-direction.

In evaluating k_N, when using round tubing, the centre line of the tubing is the classical reference diameter and is equivalent to $D_c+\delta_c$ for the square conductors that are more typical for industrial induction coils.

Induced Heating of a Cylindrical Work Piece

The classical approach for the computation of heat generation in a cylindrical work piece has been previously reviewed [5], and the resulting equations can be summarized as follows:

$$P_w = k_N^{*2}\sqrt{2}\pi(I_c N_c)^2 \rho_w \xi_w \varphi(\xi_w)/l_c \qquad (3)$$

where k_N^* is the frequency adjusted 'short coil' correction factor [unitless], ρ_w is the electrical resistivity of the work piece [Ωm], ξ_w is the dimensionless reference depth. $\varphi(\xi_w)$ a correction factor accounting for the average phase shift between current and voltage in the work piece.

$$k_N^* = k_N\left(1-\left(\frac{D_w-\delta_w}{D_c+\delta_c}\right)^2\right)+\left(\frac{D_w-\delta_w}{D_c+\ \delta_c}\right)^2 \quad (4)$$

where D_w is the outside diameter of the work piece [m], and δ_w is the electromagnetic penetration depth into the work piece [m].

$$\xi_w = \frac{D_w}{\delta_w\sqrt{2}} \quad (5)$$

$$\varphi(\xi_w) = \frac{\sqrt{2}(ber\xi_w ber'\xi_w + bei\xi_w bei'\xi_w)}{ber^2(\xi_w)+bei^2(\xi_w)} \quad (6)$$

where *ber*, *ber'*, *bei* and *bei'* are the real and imaginary parts of the zero order modified Kelvin Bessel functions and their derivatives, the solutions to which can be found using numerical solvers [4], or look-up tables [6].

$$\delta_w = \left(\frac{\rho_w}{\pi\mu_r\mu_o f}\right)^{0.5},\ \delta_c = \left(\frac{\rho_c}{\pi\mu_r\mu_o f}\right)^{0.5} \quad (7)$$

where δ is the electromagnetic penetration depth into either the work piece, *w* or coil, *c* [m], ρ is the corresponding electrical resistivity [Ωm], and *f* the frequency [Hz].

Equation (4) proposed by the present authors calculates the modified Nagaoka 'short coil' correction factor, which accounts for the effective fraction of the volume of the coil occupied by the work piece and its effect on the magnetic flux density in the air-gap, as shown in Figure 1. Equation (4) is essential for obtaining accurate magnetic field estimates when using short coils [7-9].

The impact of a work piece on the strength, curvature and location of the magnetic field produced by a short coil is indicated in Figure 1, as calculated using COMSOL 4.2® with and without a work piece.

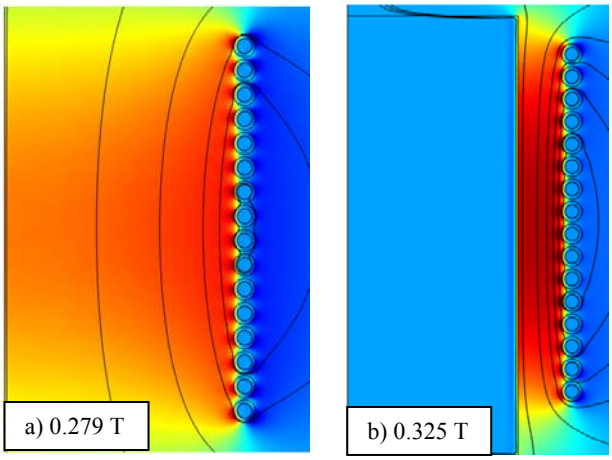

Figure 1. Peak magnetic flux density (T) for a) 'air-core' and b) 100 mm diameter, high purity aluminum work piece in a short coil (Coil #1, see Table I), at 10 kHz and 1000A RMS, indicating an ~16% increase in field strength.

Finite Element Model

Induction heating can also be estimated using modern finite element methods, as indicated previously in Figure 1. A 2D axial symmetric model of the induction heating experiments was created using the commercial code of COMSOL 4.2®. This model directly solves Maxwell's equations in the frequency domain, starting from the magnetic vector potential, A_Φ. The model equations are summarized below for a stationary system (units designated as vectors can have components in the r, phi and z directions, scalar units are indicated) [7]:

$$\vec{B} = \nabla\times\vec{A} \quad (8)$$

where *B* is the flux density [T], *A* is the magnetic vector potential [Wb/m].

$$\vec{B} = \mu_o\mu_r\vec{H} \quad (9)$$

where *H* is the magnetic field intensity [A/m].

$$\nabla\times\vec{H} = \vec{J} \quad (10)$$

where J is the current density [A/m^2] and the displacement current $\frac{\partial\vec{D}}{\partial t}$ is neglected.

$$\vec{J} = \sigma\vec{E} + \vec{J^e} \quad (11)$$

where σ is the electrical conductivity [S/m], *E* is the electric field [V/m], and J^e is the external current density [A/m^2].

$$\vec{E} = \nabla V - \frac{\partial\vec{A}}{\partial t} \quad (12)$$

where *V* is the electric potential [V] and *t* is time [s].

$$\nabla\times\vec{E} = -\frac{\partial\vec{B}}{\partial t} \quad (13)$$

In the present 2D axial symmetric model only the phi (azimuthal) components A_Φ and J_Φ are present in the magnetic vector potential $\vec{A}$ and current density $\vec{J}$. From Equations (8) to (13), the following differential equation is obtained for A_Φ assuming $\nabla V = 0$ and a sinusoidal current:

$$\frac{\partial^2 A_\phi}{\partial r^2}+\frac{1}{r}\frac{\partial A_\phi}{\partial r}+\frac{\partial^2 A_\phi}{\partial z^2}-\frac{A_\phi}{r^2} = j\omega\mu_o\mu_r\sigma A_\phi \quad (14)$$

where *j* is √-1, ω is the radial frequency (2πf) [radians/s], *r* is the radial position [m], and *z* is the axial position [m].

When A_Φ is determined, the other field quantities J_Φ, H_z, and B_z as well as the heating power can then be computed.

In a 2D axial symmetric model, a helical coil is actually modeled as a series of stacked loops. Errors in the estimated magnetic flux

density introduced by this approach are generally small (e.g. one part per thousand), and depend on the spacing and angle of the coil turns [10].

All FEM solutions presented in the results section have been calculated using current driven coils, which ensure that the correct magneto-motive force is present. The estimates of voltage and impedance in the coil domains may then have some error without causing any impact on the estimate of the induction heating in the work piece [7].

Size Requirement for the Magnetic Domain

In order to obtain accurate magnetic field estimates, it is necessary to establish the size of the 'magnetic domain', i.e. the space in which the magnetic flux may exist. If this volume is insufficient, there will be a high external magnetic reluctance, which will reduce the estimated flux density inside the coil, at any given applied current. Magnetic insulation is assumed at the boundaries of the magnetic domain, i.e. no normal component of the magnetic flux at the boundaries.

To estimate the required magnetic domain size, the inductance of a theoretical 'air core' 16 turn 'current sheet' coil was considered. This is a simple geometry for which an exact analytical solution exists for comparison. A theoretical current sheet consists of one infinitely thin turn, with the current increased to $N_c I_c$ in order to represent the number of revolutions that the current makes in a real helical coil. This 'coil' was modeled using FEM, as a single 0.1 mm thick, 105.8 mm high and 131.5 mm diameter copper sleeve, using COMSOL's single-turn domain. The model results were compared against the theoretical solution, i.e. Equation (15).

$$L_o = \frac{k_N A_c N_c \left|\overrightarrow{B_\infty}\right|}{I_c} \tag{15}$$

where L_o is the inductance of a non-infinite coil [H], and A_c is the area of the coil [m^2].

The Nagaoka coefficient for this coil (k_N) is 0.639413 and from Equation (15), its theoretical inductance is 26.4051 μH. The measured value for the experimental tubular coil of the same overall dimensions was found to be 26.902 μH including lead effects. FEM estimates were calculated as a function of the ratio of the size of the 'magnetic domain' to the size of the coil. At a ratio of 14, the FEM result was 26.4057 μH. This ratio was selected as numerically sufficient to represent an infinite external volume with a negligible error in the coil's average internal magnetic flux density [7] and was used in all subsequent FEM calculations.

Coil Domain Type and Model Mesh Requirements

In order to obtain realistic estimates of the current distributions inside of the coil tubing over all frequencies and accurate estimates of the coil impedance, it was found necessary to model the coils using COMSOL's single-turn domain. The multi-turn domain assumes a homogenous current distribution and does not give accurate results for frequencies where the electromagnetic penetration depth is smaller than the wall thickness, i.e. $\delta_e < t_c$ [7].

At high frequency it was required to mesh the coil and work piece with boundary meshes, such that the mesh spacing was less than the thickness of their respective electromagnetic penetration depths as given by Equation (7). Failure to adjust the mesh spacing, resulted in errors as high as 73% in the FEM estimates of heating at very high frequencies [7]. It is obvious that a fine mesh is required to obtain satisfactory spatial resolution of the magnetic field and current in the first electromagnetic penetration depth or 'shell' thickness due to the very steep local gradients.

Electrical Conductivity

In order to model induction heating, the electrical conductivity at the work piece temperature (or its inverse, resistivity), is the most important material property. The electrical conductivity of the aluminum work pieces were measured using a General Electric Inspection Technologies, UK (AutoSigma 3000) conductivity analyzer to within ±0.5% accuracy, calibrated against aluminum standards accurate to ±0.01% IACS (International Annealed Copper Standard [11]). The electrical conductivity was not used as a fitting parameter in either the analytical or FEM modeling approaches.

In order to estimate the electrical conductivity or resistivity at the elevated operating temperatures of the experiments, Equations (16) to (18) are required. It is most convenient to work in resistivity units, as it results in a linear correlation with temperature as indicated by Equation (16):

$$\rho = \rho_o \left(1 + \alpha_{293}\left[T - 293K\right]\right) \tag{16}$$

where ρ is the resistivity of either the coil or the work piece, ρ_o is the resistivity of the metal at reference temperature T [Ωm], α_{293} the temperature coefficient of resistivity [K^{-1}], and T the reference temperature (293 [K]). The following values are recommended: for 100% IACS copper, ρ_o = 1.7241E-8 Ωm (58.00 MS/m) and α_{293} = 0.00393 [11]. For 99.99% purity well annealed aluminum, ρ_o = 2.650E-8 Ωm (65.0% IACS) and α_{293} = 0.0043 (for temperatures between 293 and 673 K) [12].

Electrical resistivity, ρ_o, of an alloy can be found from the measured %IACS conductivity by:

$$\rho_o \textit{ for Alloy XXXX} = \rho_{o\ (\textit{for 100\% IACS copper})} * 100 \,/\, \%\textit{IACS for Alloy XXXX} \tag{17}$$

For aluminum alloys, a new equation is proposed here based on comparison with available literature data [13-15], to estimate the temperature coefficient of resistivity:

$$\alpha_{20} \textit{ for Alloy XXXX} = \frac{0.0043(\textit{AlloyXXXX\%IACS})}{65.0} \tag{18}$$

Combining Equations (16) through (18), the resistivity as a function of temperature of an aluminum sample can be estimated for temperatures between 293 and 673 K, from a single reading of %IACS conductivity measured at room temperature.

Experimental Conditions and Procedures

Table I summarizes the coil and work piece data used in the experiments. Heating and magnetic field measurements were collected using insulated and water cooled work pieces, as shown in Figure 2 for long Coil #3 and Work piece #3. Work pieces were precisely machined to remove the less representative outer layers (i.e. grain structure and electrical conductivity). Coil and work piece data have been summarized in detail elsewhere [8-9].

Thermal heating measurements were made while applying a constant voltage to the coil and simultaneously measuring the temperature and flow rate of the water into and out of the work piece and current flowing in the coil. When both electrical and thermal stability had been reached, a number of electrical measurements were carried out over a period of about 5-20 minutes.

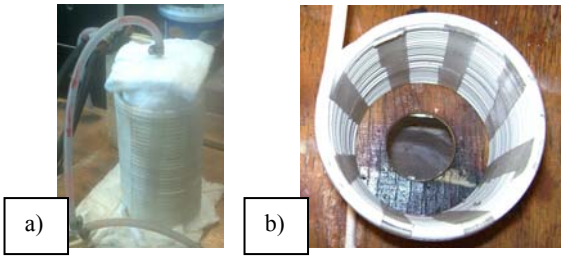

Figure 2. a) Insulated and water cooled 6060 aluminum Work piece #3 in long Coil #3, b) top view of long Coil #3.

Table I. Data for Coil #1, Coil#3 and Work Pieces #1 and #3 [8]

Work Pieces	**1**	**3**
Alloy	A356	6060
Diameter, mm	75.0	95.0
Length, mm	130.0	260.0
Measured IACS Electrical Conductivity, %	48.4	53.4
Penetration Depth δ_w (mm) at 50 Hz and 293 K	13.43	12.79
ξ_w	3.948	5.252
$\varphi(\xi_w)$	0.823	0.859
Coil 1	1-1	
Coil 3		3-3
Coils	**Short Coil 1**	**Long Coil 3**
Average Diameter, mm	132	132
Height, mm	106	218
Diameter to Height ratio	1.24	0.60
Number of Turns	16	32
Short Coil Correction Factor	0.641	0.786
Electrically Determined IACS Conductivity, %	80	80
Penetration Depth δ_c (mm) at 50 Hz and 293 K	10.45	10.45
Modified Nagaoka Coefficient k_N* for Work Piece 1	0.720	
Modified Nagaoka Coefficient k_N* for Work Piece 3		0.870

The thermocouples used were 'matched' to give the same temperature readings at room temperature, such that the precision error in the delta-temperature, was on the order of ±0.05°C. This represented an uncertainty in the thermal measurements of ~2%. Based on the amount and type of the thermal insulation used, heat losses averaged ~0.4% [8-9].

Power measurements were taken using a power analyzer from Fluke, USA (Fluke 43B), with a resolution of ±100W. Coil current measurements were made with an inductive current probe from Fluke, USA (i1000S), with an accuracy of ±1% and a resolution of 1A. Electrical data represent the average of between 2 and 8 readings.

Water flow rate was determined using a scale which had a capacity of 100 kg and a resolution of 0.01 kg. The total weight difference over the period of each power reading was then used to calculate the average flow, which therefore had <0.1% error.

The direct measurements of the magnetic flux density of short Coil #1 in the present study were taken using a Pacific Scientific OECO, USA (F.W. Bell model 6010 Gauss meter). Standardized axial and radial Hall probes, with a measuring error of less than ±1% for AC magnetic fields were used. The accuracy was confirmed using axial standards of 0.05 and 0.2 T, and a transverse standard of 0.05 T, prior to use of the probes.

Magnetic Field of an 'Air Core' Coil

A short empty or 'air core' coil does not have a homogeneous magnetic field in either the axial or radial directions. Along the central axis of an empty coil it is possible to determine the variation of the flux density in the z-direction using the Biot-Savart law. A solution of the Biot-Savart law, as a function of the dimensionless coil position, x, is shown below [8]:

$$\left|\overline{B_o}\right| = \frac{\mu_o N_c I_c}{2 l_c}\left(\frac{x l_c}{\sqrt{(x l_c)^2 + r_c^2}} + \frac{(1-x) l_c}{\sqrt{((1-x) l_c)^2 + r_c^2}}\right) \qquad (19)$$

where x is the dimensionless coil length measured from one end of the coil, and r_c is the effective radius of the coil taken from the coil axis to the tubing centre line for round tubing, i.e. $2\, r_c = D_c + \delta_c$ [m].

A number of magnetic field measurements have been taken to validate the accuracy of the FEM model for its later use in the prediction of heating rates [8]. In Figure 3, axial experimental data for empty short Coil #1 are plotted together with the solution to Equation (19) for a coil diameter to length ratio of 1.24. Results have been normalized by dividing the calculated and measured results by Equation (1).

The measurements of the z-component of the magnetic flux density were taken with a 6 mm diameter axial Hall probe. The plotted results allow for the average 3 mm off-set. Results from Equation (19) are marked with stars, estimates from FEM are marked with various lines and the experimental data are marked with different markers. It should be noted that on the centre-line, that the agreement between FEM and the Bio-Savart Equation (19) is so exact, that the data are directly over each other, making them difficult to distinguish.

Magnetic Field of a Coil Containing a Work Piece

Magnetic field measurements were also taken with short Coil #1 operating with and without the A356 aluminum Work piece #1 and results are plotted in Figure 4. FEM estimates are plotted as lines at a radius of 40.5 mm for Coil #1 operating with an air-core

and with Work piece #1. Experimental data for both the air-core and coil with work piece are plotted using markers. The relative increase in the magnetic field strength caused by the presence of the work piece is indicated by the arrows.

From Figures 3 and 4 the following observations can be made:

- The expected variation of the magnetic flux density in both the radial and axial directions is clear from Figure 3.
- The reproducibility of the measurements is good, as evidenced by the multiple data sets plotted in Figures 3.
- The increase in the magnetic flux density caused by the insertion of a work piece and predicted by Equation (4) is evident in Figure 4.
- The agreement between experimental values and the 2D axial symmetric FEM model estimates is excellent (±1-4% with an average error of ±2%).

The errors in the magnetic flux density measurements were slightly higher at the ends of the coils, where they are least 'axial' symmetric. Based on the thermal measurements reported elsewhere [8-9], agreement of ±1-2% was expected between the measured values and FEM estimates (square root of the difference in power). The slightly higher experimental discrepancies are likely to be the result of geometric positioning errors (+/- 0.5-1.0 mm and angular alignment) as well as the non-axial symmetry of the experimental coil.

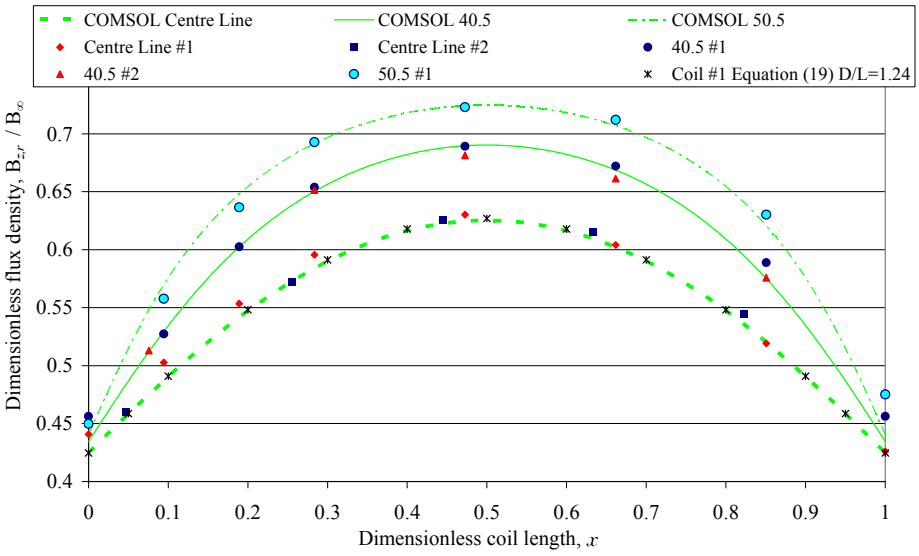

Figure 3. Magnetic flux density (z-component) measurements using short Coil #1, including duplicates [8].

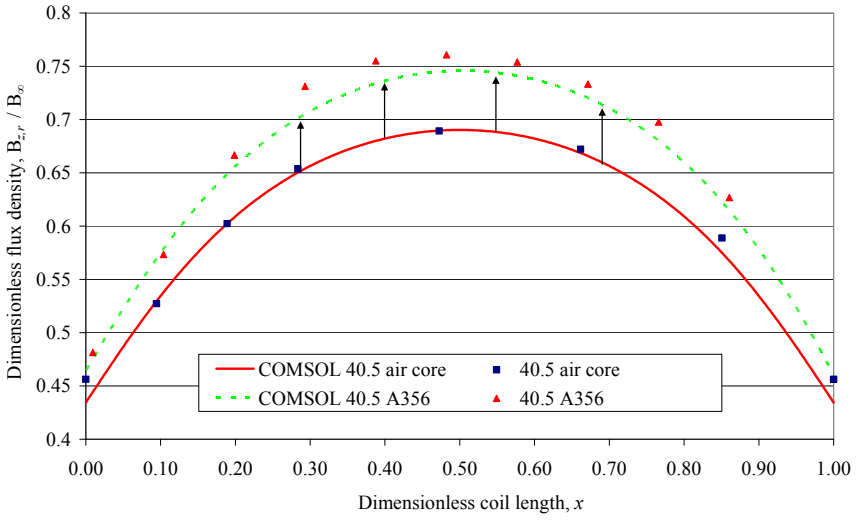

Figure 4. Magnetic flux density (z-component) in short Coil #1, with and without Work piece #1 [8].

Measurement and Estimation of Heating Rate

In the previous section, the magnetic field predictions of COMSOL 4.2® were validated against both analytical and experimental solutions with and without a work piece at 50 Hz. Further validation has been accomplished by way of heating rate (power) comparisons between experimental data, analytical and FEM estimates at 50 Hz. Good agreement has been found, showing approximately 2% difference between the FEM estimates and the calorifically determined values. Differences of 3-5% were found between the experimental data and the analytical estimates obtained from Equations (3) to (7) depending on the data sets used for comparison [8-9].

In order to explore the reliability of the FEM and analytical model estimates, comparisons are shown in Table II for Work piece #1 and short Coil #1 and Table III for Work piece #3 and long Coil #3, covering both the experimental values at 50 Hz and a wide range of frequencies up to 500 kHz.

Table II. Comparison between the Estimates of Heating (Power) as a Function of Frequency for Short Coil #1 and Work Piece #1, at 1001 A, ρ_w =3.76 x10^{-8} Ωm [8-9]

Frequency (Hz)	Thermal Experimental Power (W)	Electrical Experimental Power (W)	Analytical Power (W)	COMSOL Power (W)	Analytical-COMSOL Difference (%)
50	634	611	659	623	5.8
500	N/A	N/A	2567	2466	4.1
5000	N/A	N/A	8672	8370	3.6
50000	N/A	N/A	27957	26816	4.3
500000	N/A	N/A	88623	85247	4.0
				Average:	4.3

Agreement between the Thermal data and the Electrical, Analytical and COMSOL estimates is very satisfactory for the long Coil #3 and Work piece #3. The bias between the FEM and analytical estimates is 0.5% (note that the absolute error is shown in Table III) for the long Coil #3. Coil #3 being approximately twice the length of Coil #1, is more 'ideal' and therefore Equation (4) applies less correction to account for the presence of the work piece. A proportionately larger bias of 4% was found between the FEM and analytical estimates for the short Coil #1 and Work piece #1 [8-9]. The variation of bias with coil and work piece geometry is probably due to the empirical nature of Equation (4).

Table III. Comparison between the Estimates of Heating (Power) as a Function of Frequency for Long Coil #3 and Work Piece #3, at 558 A, ρ_w =3.30 x10^{-8} Ωm [8]

Frequency (Hz)	Thermal Experimental Power (W)	Electrical Experimental Power (W)	Analytical Power (W)	COMSOL Power (W)	Analytical-COMSOL Difference (%)
50	736	727	722	713	1.3
500	N/A	N/A	2660	2616	1.7
5000	N/A	N/A	8739	8704	0.4
50000	N/A	N/A	27762	27844	0.3
500000	N/A	N/A	87920	88348	0.5
				Average:	0.8

From 500 Hz, the data in Table III show the expected high frequency relationship, i.e. heating rate becomes proportional to √frequency.

If Equation (4) were not used to correct for the shortness of the coil and the presence of the work piece in the analytical estimates of the heating rate, an error of 98% would result for Work Piece #1 and short Coil #1 and an error of 34% for Work piece #3 and long Coil #3.

The heat input to the work piece should vary in proportion to the square of the local magnetic flux density. As previously shown in Figure 4, a significant axial gradient exists in the local magnetic flux density at the surface of the work piece. The square of the measured local magnetic flux density in dimensionless form has been plotted against the FEM estimate of the surface heating rate in Figure 5, as a function of dimensionless coil length. Agreement is very reasonable.

Conclusions

Accurate (experimental) measurements and comparison with analytical solutions has allowed for precise validation of the COMSOL 4.2® 2D axial symmetric FEM model. Excellent agreement was achieved between experimental data and model estimates of both the magnetic flux density and heating (power) at 50 Hz. Analytical and FEM model heating estimates were in consistent agreement at frequencies from 50 Hz to 500 kHz. The modified 'short coil' correction factor was a key factor in obtaining accurate analytical model predictions. A new method of correlating the resistivity temperature coefficient has been presented for use with aluminum and its alloys.

Acknowledgements

The present study was carried out as part of the RIRA (Remelting and Inclusion Refining of Aluminium) project funded by the Norwegian Research Council (NRC) - BIP Project No. 179947/I40. The industrial partners involved in the project are: Hydro Aluminium AS, SAPA Heat Transfer AB, Alcoa Norway ANS, Norwegian University of Science and Technology (NTNU) and SINTEF Materials and Chemistry. The funding granted by the industrial partners and the NRC is gratefully acknowledged.

The authors wish to express their gratitude to Egil Torsetnes at NTNU for helping with the design and construction of the experimental apparatus. Sincere gratitude is also due to Kurt Sandaunet at SINTEF for his support and help, as well as for the use of the SINTEF laboratory.

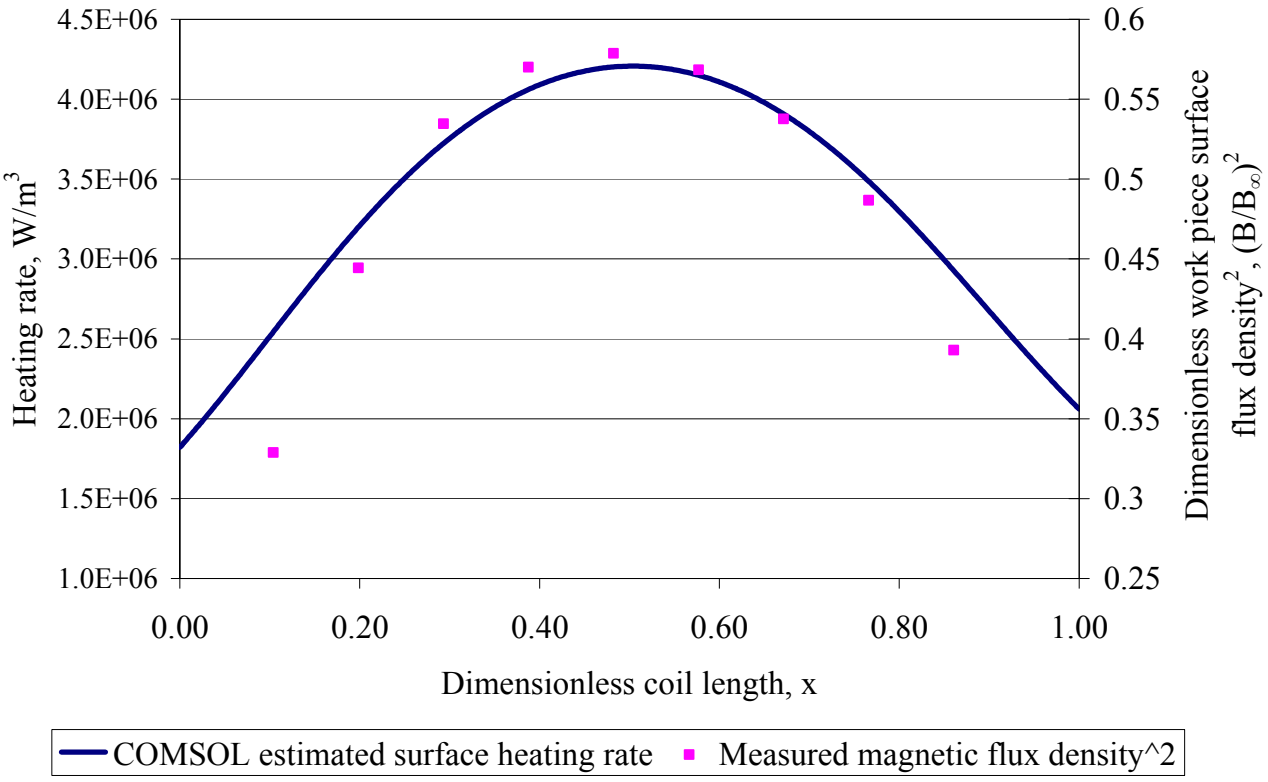

Figure 5. Comparison between local measured magnetic flux density squared and the FEM estimate of surface heating rate for short Coil #1 and Work piece #1, as a function of axial position, at 1001 A and 50 Hz.

References

1. H. Nagaoka, "The Inductance Coefficients of Solenoids," *Journal of the College of Science,* 27, (1909), 18-33.
2. L. Lorenz, "Ueber die Fortpflanzung der Electricität," *Annalen der Physik,* 243, (1879), 161-193.
3. D. Knight, http://www.g3ynh.info/zdocs/magnetics/part_1.html, September 22, (2011), [Online].
4. R. Weaver, http://electronbunker.sasktelwebsite.net/DL/NumericalExamples01.ods, September 22, (2011), [Online].
5. M. W. Kennedy, S. Akhtar, J. A. Bakken, and R. E. Aune, "Review of Classical Design Methods as Applied to Aluminum Billet Heating with Induction Coils," EPD Congress, San Diego, California, February 27 - March 3, (2011), 707-722.
6. N. McLachlan, *Bessel Functions for Engineers*, (Gloucestershire: Clarendon Press, 1955).
7. M. W. Kennedy, S. Akhtar, J. A. Bakken, and R. E. Aune, "Analytical and Experimental Validation of Electromagnetic Simulations Using COMSOL®, re Inductance, Induction Heating and Magnetic Fields," Submitted to the COMSOL Users Conference, Stuttgart Germany, October 26-28, (2011).
8. M. Kennedy, S. Akhtar, J. A. Bakken, and R. E. Aune, "Theoretical and Experimental Validation of Magnetic Fields in Induction Heating Coils," submitted to *IEEE Transactions on Magnetics,* (2011).
9. M. Kennedy, S. Akhtar, J. A. Bakken, and R. E. Aune, "Improved Short Coil Corection Factor for the Induction Heating of Billets," Submitted to the EPD Congress, Orlando Florida, March 11-15, (2012).
10. C. Snow, "Formula for the Inductance of a Helix Made with Wire of Any Section," US Govt. Print. Off., 1926, 1-91.
11. *Copper Wire Tables Circular No. 31*: US Bureau of Standards, (1913).
12. P. Desai, H. James, and C. Ho, "Electrical Resistivity of Aluminum and Manganese," *Journal of Physical and Chemical Reference Data,* 13, (1984), 1131-1172.
13. R. Brandt and G. Neuer, "Electrical Resistivity and Thermal Conductivity of Pure Aluminum and Aluminum Alloys up to and Above the Melting Temperature," *International Journal of Thermophysics,* 28, (2007), 1429-1446.
14. S. Bakhtiyarov, R. Overfelt, and S. Teodorescu, "Electrical and Thermal Conductivity of A319 and A356 Aluminum Alloys," *Journal of Materials Science,* 36, (2001), 4643-4648.
15. T. C. Totemeier and C. J. Smithells, *Smithells Metals Reference Book*: (Butterworth-Heinemann, 2004).